Progress In Electromagnetics Research C, Vol. 113, 211–226, 2021

A Compact Low SAR and High Gain Circularly Polarized AMC Integrated Monopole Antenna for WBAN Applications

Nibash K. Sahu* **and Sanjeev K. Mishra**

Abstract—This paper presents a compact CPW fed circularly polarized AMC integrated monopole antenna with low SAR and high gain for 2.4 GHz WBAN applications. The proposed design is achieved through a four-stage progression. Stage-1 consists of a straight monopole with an extended vertical stub at one of the ground planes to generate circular polarization. In Stage-2, a novel 3×3 ring-type isotropic AMC is implemented beneath the monopole antenna to mitigate the antenna's back radiations towards the human body. On the body at '0' mm distance, it reduces the SAR by 99.47% and increases the impedance bandwidth, radiation efficiency, and gain to 480 MHz, 77%, and 7.1 dBi, respectively. However, there is a decrease in AR bandwidth that indicates AR $>$ 3-dB, which is compensated in Stage-3 by optimizing the monopole. The optimization results in an AR BW of 190 MHz and a size reduction of monopole antenna by 30.862%. Due to the size reduction of monopole with same AMC, the SAR reduction and peak gain are improved to 99.63% and 7.4 dBi, respectively. In Stage-4, the 3×3 AMC is replaced by 2×2 AMC, resulting in the total size and SAR reduction of 55.56% and 97.72%, respectively. Stage-4 provides a simulated impedance bandwidth of 350 MHz, peak gain of 6.4 dBi and AR bandwidth of 170 MHz, whereas the fabricated structure on felt substrate provides 650 MHz, 6.5 dBi, and 150 MHz, respectively.

1. INTRODUCTION

Wireless body area network (WBAN) has gained growing popularity in recent years due to its potential applications in sports, health care, military, public safety, and consumer fitness fields. In such demand of WBAN, wearable antenna is a key component due to the wireless communication with other devices on or off the human body. It may communicate with other antennas on the body's surface (on-body communication) or with an external antenna (off-body communication). The latter mode of communication necessitates a broad side radiation pattern. To be used for body-worn application, an antenna must have certain characteristics such as high gain, high efficiency, low specific absorption rate (SAR), and also be flexible on the body [1, 2].

Two major challenges in developing wearable antennas are preserving performance under bending condition and minimizing the negative impact of antenna's contact with dissipative biological tissue. To begin, the operating frequency can become detuned as a result of various bending conditions caused by body curvature or movement. In this case, a wide band antenna is the best option, as it can cover the appropriate band even if the resonance frequency shifts due to bending. Monopole antennas are widely used in literature because they can be easily tuned to achieve wide band operation and also provide compactness and flexibility, making them excellent candidates for wearable WBAN applications. The materials used for flexibility are textiles [3–9], polyimides [10–19], polyester film [20], papers [21, 22], and latex [23]. The second challenging aspect which is most important for researchers is taking care of electromagnetic (EM) radiation effects on the human body. Human body is highly lossy and dispersive material with high dielectric constants, which absorb a significant amount electromagnetic energy

Received 17 May 2021, Accepted 23 June 2021, Scheduled 30 June 2021
* Corresponding author: Nibash Kumar Sahu (nibash11@gmail.com).
The authors are with the Department of International Institute of Information and Technology, Odisha 751003, India.

radiated by antenna. As a result, it is very common for the antenna gain that decreases significantly when the antenna is operated in close proximity to human body. In addition, the body absorbed EM energy may cause unwanted, adverse biological effects. Therefore, US Federal Communications Commission (FCC) [24] and EU commission regulations [25] restrict the SAR to 1.6 W/kg and 2 W/kg averaged over 1 g and 10 g tissue, respectively. In order to reduce the SAR, separation is kept between human body and antenna. Mainly, two methods are used to separate the human body from antennas which are shielding the antenna from body by using perfect electric conductor (PEC) and artificial magnetic conductors (AMCs). The works reported in [3, 26–30] demonstrated that antennas with a back shield ground plane could provide a desire to minimize the radiation backward, increase the stability of the wearable antenna, and isolate the human body from electromagnetic radiations. Nevertheless, utilizing PEC as backing reflectors, the reflected waves are out-of-phase with incident waves [31]. As a consequence, destructive interference occurs, so overall performance degrades. In addition, maximum energy is stored in between antenna and reflector with low radiation. To solve these issues, the most commonly used technique is using AMC or electromagnetic bandgap (EBG) between human body and antennas [4, 7, 19, 31–36]. AMC typically provides high impedance surface (HIS) which exhibits in-phase reflection phase with incident waves (incoming waves). Hence, the antenna performances such as low SAR, high efficiency, high gain, and high front to back ratio with minimization of the back radiation towards the body are achieved. However, the above reported works provide linear polarization in the 2.4–2.4835 GHz industrial, scientific, and medical (ISM) band. So far, almost all the wearable antennas proposed for ISM band provide linear polarization (LP). To date, very few CP antennas have been reported for OFF-body WBAN applications. CP antennas are advantageous over linearly polarized antennas in terms of link reliability, especially in dynamic channels where the orientation of the antenna is unfixed [37]. Circularly polarized (CP) radiation provides the antennas better resistivity against polarization mismatch and multipath interference. The authors of [38] demonstrated a coplanar waveguide (CPW) fed monopole antenna which provided bidirectional radiation patterns. However, bidirectional radiation pattern absorbs a considerable amount of energy. In [12, 28–30], circular polarization with unidirectional radiation patterns has been achieved at ISM band.

Accordingly, this paper presents a compact, wide band, circularly polarized, low SAR, high gain, and high efficient wearable antenna operating in 2.4 GHz ISM band for the sports application such as monitoring and recording the medical status and performance. As a result, the proposed antenna is intended to be worn on the back side of human body. The following characteristics distinguish the proposed study from previous circularly polarized unidirectional antennas:

- In [12], x-polarized wave was incident on an anisotropic artificial ground plane to generate y-polarized reflected wave, and then the two were combined at far fields to result in a circularly polarized wave. In this work, a circularly polarized wave was incident on an isotropic artificial ground plane to get a circularly polarized wave at far-field.
- In [28, 29], truncated cornered microstrip antennas with ground shield were proposed for achieving circular polarizations and unidirectional radiation patterns, respectively. However, they provided narrow impedance bandwidth, and because of large ground plane, the total footprints were large, and thus frequency detune occurred during bending. Therefore, in this work monopole antenna was presented which provided wide impedance bandwidth with smaller size than a microstrip antenna.
- In [30], a CPW fed-straight monopole with an additional stub and a PEC reflector made of high permittivity substrate was used for achieving circular polarization and unidirectional radiation pattern, respectively. In order to achieve constructive interference, the authors implemented the PEC at quarter wave length distance of approximately 13 mm at 5.8 GHz ISM band. However, at 2.4 GHz, this distance would increase to about 31 mm which would significantly increase the total foot prints and also make the flexibility of antenna more challenging. As a result, an AMC reflector was used in this work at a distance of 0 mm from the radiators, which resulted in a compact size and ease of flexibility.

This paper is organized as follows. The structure and characteristic of the AMC plane are introduced and analyzed in Section 2, prior to the evolution of compact AMC integrated antenna in Section 3. Section 4 discusses the antenna performance in free space and on-body with a comparison of proposed work and existing works, and finally, Section 5 concludes the proposed design for the WBAN application.

2. CHARACTERISTIC OF AMC PLANE

Figure 1(a) shows the topology of a single AMC unit cell. The ring type structure is used as single unit cell in this design. The AMC is fabricated on 3 mm thick felt substrate with dielectric constant 1.63 and loss tangent 0.044 [41]. The AMC structure consists of three layers where an array of periodic ring cells is on the top layer, substrate on the middle, and ground on the bottom layer. The size of each unit cell is 27 mm, and period is 28 mm. The conducting part is made using copper sheets. The single cell is simulated using CST Microwave Studio by assigning unit cell boundaries and Floquet port to mimic the infinite planer periodicity. In order to characterize the reflection phase, x-polarized and y-polarized plane waves are incident from the normal direction. The reflection phase characteristic is shown in Fig. 1(c). The phase of the reflected wave for x-polarization and y-polarization is 0° at 2.45 GHz, and hence AMC exhibits a perfect magnetic conductor (PMC) like characteristic. The operating bandwidth of proposed AMC that is frequency range of phase in between −90° and 90° is 388.6 MHz (2.2557–2.6443 GHz). The advantage of using ring type AMC instead of square patch type is that ring type can provide smaller size as compared to square type patch at the same operating frequency. For validation, the square patch with same material, size and thickness as shown in Fig. 1(b) is also simulated. It is observed that the proposed AMC provides 0° reflection phase at 2.45 GHz while square AMC is at 2.788 GHz. Hence, miniaturization is achieved by using a ring type AMC. Table 1 lists the dimensions of square type and ring type unit cells.

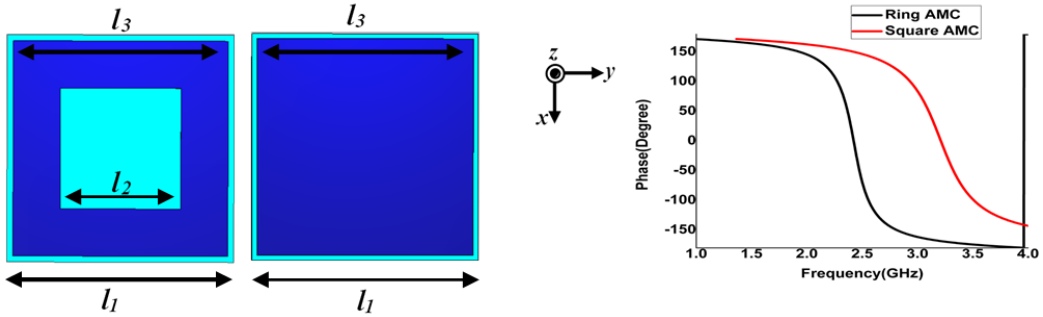

(a) (b) (c)

Figure 1. Structure of (a) ring type AMC, (b) square type AMC and (c) reflection phase diagram for ring-type AMC and square-type AMC.

Table 1. Dimensions of ring and square type of unit cell.

Parameter	Ring type cell	Square type cell
l_1 (mm)	28	28
l_2 (mm)	15.13	NA
l_3 (mm)	27	27

3. ANTENNA DESIGN

Figure 2 shows the structure of complete evolution of Stage-1 to Stage-4 via Stage-2 and Stage-3 to achieve compactness, circular polarization, high gain, and high efficiency. The dimension of evolution parameters is tabulated in Table 2. Flexible felt material of thickness 1.5 mm with $\varepsilon_r = 1.63$ and $\tan\delta = 0.044$ is taken as the substrate [41]. Here, CPW feeding technique is used to excite the antenna. The advantage of using CPW-feed is to place it in close proximity to the human body surface as compared to bottom fed topologies that have been considered in reported CP wearable patch antennas [28, 39, 40].

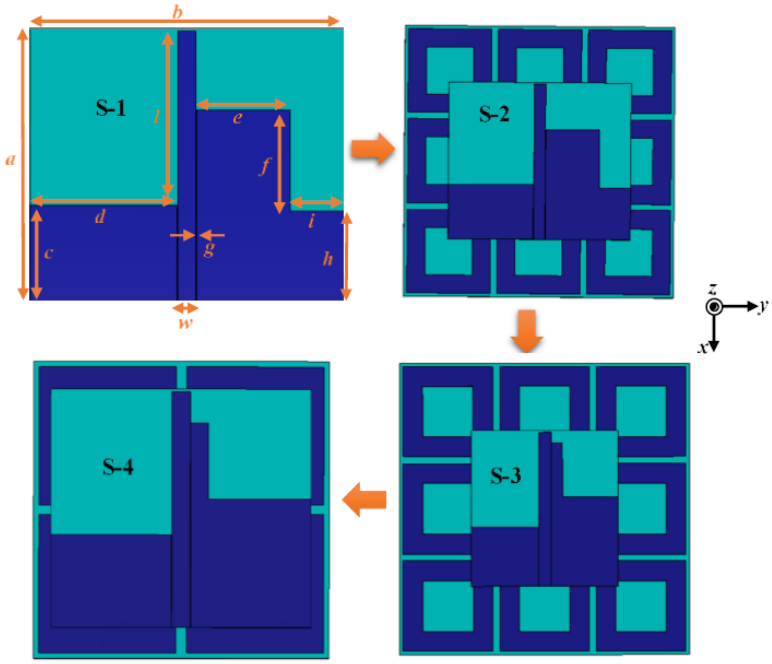

Figure 2. Structure for the evolution of Stage-1 (S-1)- Stage-2 (S-2)- Stage-3 (S-3)- Stage-4 (S-4).

Table 2. Dimensions of the evolutions from Stage-1 to Stage-4.

Antenna	$a/b/c/d/e/f/g/h/i/l/w$ (mm)	Size of AMC
Stage-1	50.5/58.6/17.6/27.45/17.5/18.8/0.1/16.6/9.95/32.9/3.5	NA
Stage-2	50.5/58.6/17.6/27.45/17.5/18.8/0.1/16.6/9.95/32.9/3.5	3×3
Stage-3	46.5/44/18/20.15/3.5/16/0.1/27/16.65/28.9/3.5	3×3
Stage-4	46.5/51/18/23.65/3.5/15/0.1/25/20.15/28.9/3.5	2×2

In Stage-1, a circularly polarized monopole antenna with a resonance frequency close to that of the AMC is targeted. The choice of such near resonance frequency is intended to achieve a broad impedance bandwidth. As illustrated in Figure 3, the first phase of Stage-1 is to design a quarter wavelength CPW fed linearly polarized monopole antenna at 2.4 GHz using CST Microwave Studio. Table 3 summarizes the dimensions. To achieve circular polarization, orthogonal modes are generated by introducing a vertical stub on the right side ground plane. According to [30], parameters 'c', 'e', 'f', and 'h' are important parameters for controlling the resonant frequency and axial ratio curve as shown in Figure 2. Parameters 'c', 'e', 'f', and 'h' are chosen properly to design a circularly polarized monopole antenna operating at 2.4 GHz, and their dimensions are tabulated in Table 2. To reduce the back radiation, in Stage-2, a 3×3 array square loop AMC reflector is implemented beneath the monopole antenna as shown in Figure 2. A 3 mm foam is utilized as spacer between the monopole antenna and AMC to avoid any electrical contact and thereby prevent short circuit. The foam is modeled in simulation by creating a rectangular box with ε_r of 1.08 and $\tan\delta$ of 0.008 [7]. However, in Stage-2, the axial ratio curve is detuned by shifting its dip to higher frequency band and upward. Thus, to achieve circular polarization at ISM band, in Stage-3, the monopole antenna is optimized by changing the dimensions of 'd', 'c', 'e', 'l', and 'f' as follows:

- Initially, the parameter 'd' of Stage-2 is reduced to 20.15 mm to bring the dip of axial ratio closer 0 dB, which automatically reduces 'b' to 44 mm.
- Then by increasing parameter 'h' to 27 mm, the dip in axial ratio is tuned toward lower frequency.
- After tuning the dip of AR curve to lower frequency band, 'e' is reduced to 3.5 mm to improve the

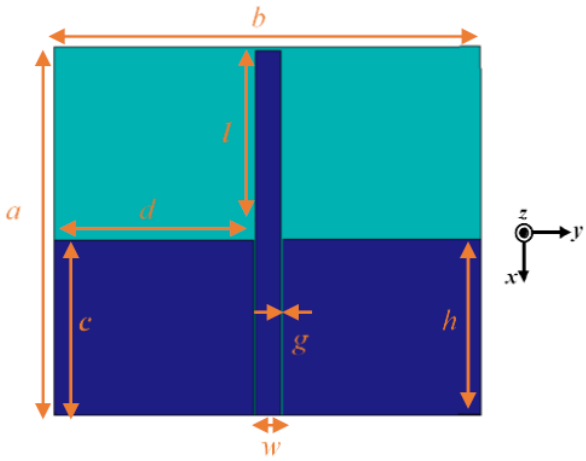

Figure 3. Structure of the linearly polarized CPW fed monopole antenna.

Table 3. Dimensions of the linearly polarized monopole antenna.

$a/b/c/d/g/h/l/w$ (mm)
50.5/58.6/24/27.25/0.3/24/26.5/3.5

resonance performance and hence impedance bandwidth.

- Then length of monopole ('l') is reduced to 28.9 mm to shift the resonant frequency to higher frequency.
- Finally, the length of stub ('f') is slightly reduced to 16 mm to obtain the optimized antenna for Stage-3, resulting in increasing the dip of reflection coefficients with circular polarization in ISM band.

The optimization of the monopole antenna results in an increase of peak gain and decrease of SAR. Finally in Stage-4, the 3×3 AMC is replaced by a 2×2 AMC to make more compact to overall foot prints. The extended ground with stub is used for orthogonal mode generations, and AMC for the reduction of back radiation, which distinguish the proposed work from [30].

4. RESULTS AND DISCUSSIONS

4.1. Free Space Performance

Figure 4 shows the reflection coefficient, gain vs frequency and radiation efficiency of the linearly polarized monopole antenna. It provides an impedance bandwidth of 430 MHz, radiation efficiency of 90%, and gain of 2 dBi at 2.4 GHz. Figures 5 and 6 depict the reflection coefficient and axial ratio for Stage-1 to Stage-4, respectively. Stage-1 provides a broad impedance bandwidth of 310 MHz (2.26 GHz–2.56 GHz) with a wide 3 dB axial ratio bandwidth (830 MHz). After introducing 3×3 AMC in Stage-2, the impedance bandwidth is enhanced to 480 MHz (2.19 GHz–2.65 GHz). However, the dip of the axial ratio is detuned and shifted toward higher frequency band with dip more than 4 dB as shown in Figure 6(b). The AR deviation might be due to the creation of mutual coupling between the monopole antenna and AMC. To get the 3-dB axial ratio (AR) bandwidth (BW) in ISM band, the monopole antenna is optimized. The reflection coefficient and axial ratio for the optimization parameters are shown in Figure 7. It is observed that the dip of the axial ratio moves downward to 1.18 dB at 2.7 GHz, and reflection coefficient moves upward due to the reduction of the parameter 'd'. After that, by increasing the parameter 'h', the axial ratio dip shifts to 2.45 GHz. However, the impedance bandwidth is affected. Then, the reduction of the stub width ('e') results in the improvement of impedance

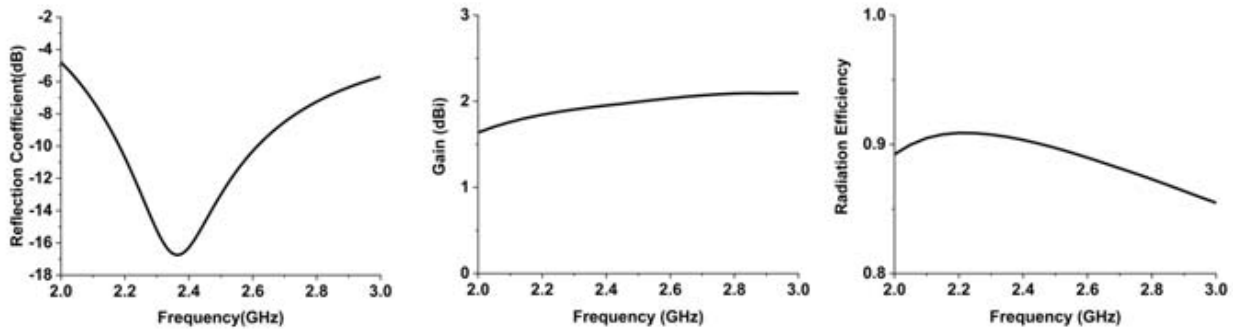

Figure 4. (a) Reflection coefficient, (b) gain vs frequency, and (c) radiation efficiency of linearly polarized monopole antenna.

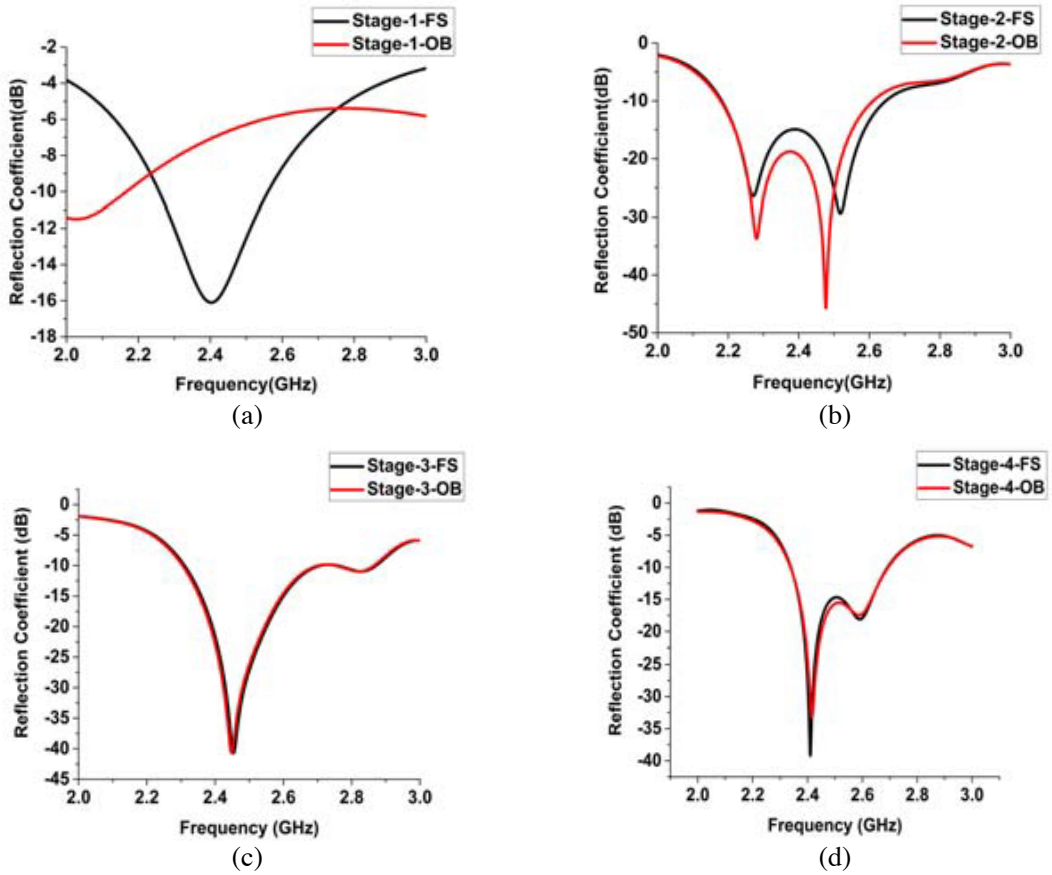

Figure 5. Reflection coefficient vs frequency in free space and on body for (a) Stage-1, (b) Stage-2, (c) Stage-3, and (d) Stage-4.

bandwidth associated with a lower resonant frequency at 2.35 GHz. The AR curve is affected. Thus, to shift the resonant frequency to 2.4 GHz, the length of monopole ('*l*') is reduced, resulting in an increase of impedance bandwidth. Here the dip of axial ratio curve occurs at 2.4 GHz. After that, the length of stub is decreased, which shifts the dip of axial ratio to 2.45 GHz with increased resonant frequency dip and impedance bandwidth. The optimization reduces the size of monopole antenna by 30.862%. Stage-3 provides a 3-dB AR BW and an impedance BW of 190 MHz (2.37–2.56 GHz) and 430 MHz (2.3–2.73 GHz), respectively. Furthermore to reduce the overall foot prints, the 3×3 AMC is

substituted by a 2×2 AMC in Stage-4 which shows a 55.56% reduction of overall foot print. However, the AR dip shifts slightly toward the higher frequency, which is retained by a slight increase of ground plane width. Stage-4 provides an impedance BW of 350 MHz (2.35 GHz–2.7 GHz) with an AR BW of 170 MHz (2.34 GHz–2.51 GHz).

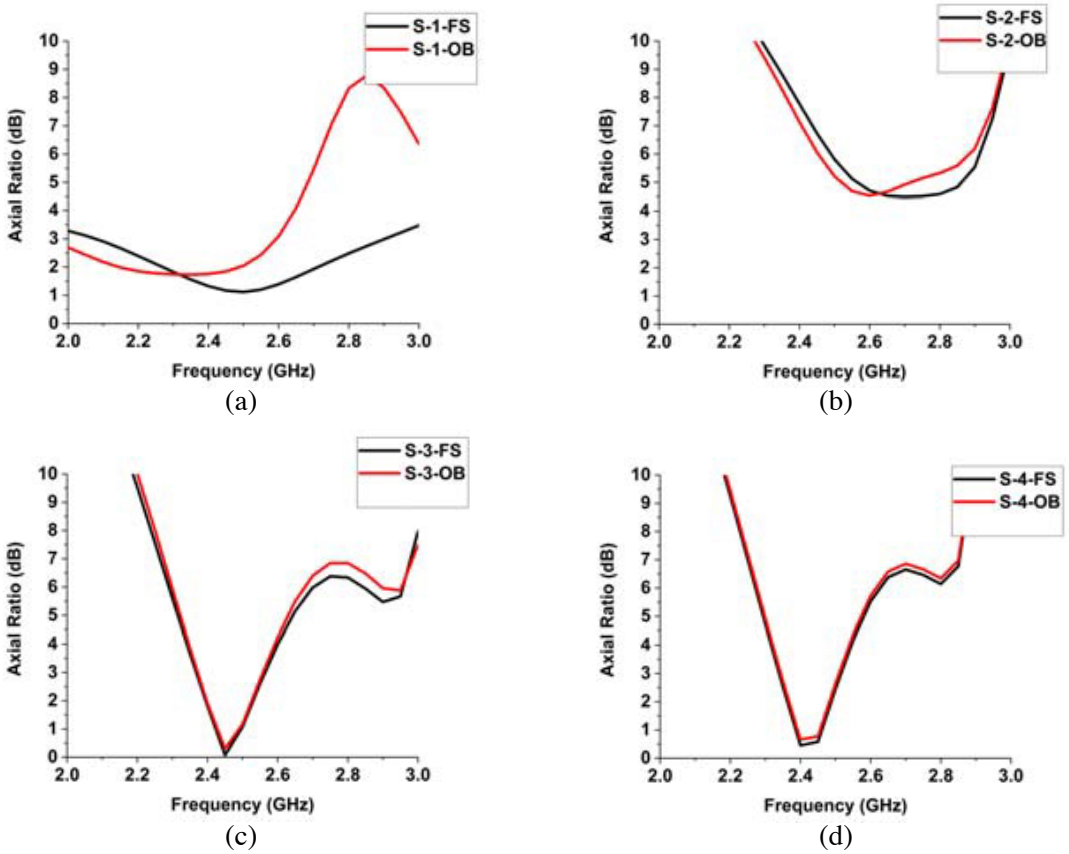

Figure 6. Axial Ratio vs frequency in free space and on body for (a) Stage-1, (b) Stage-2, (c) Stage-3, and (d) Stage-4.

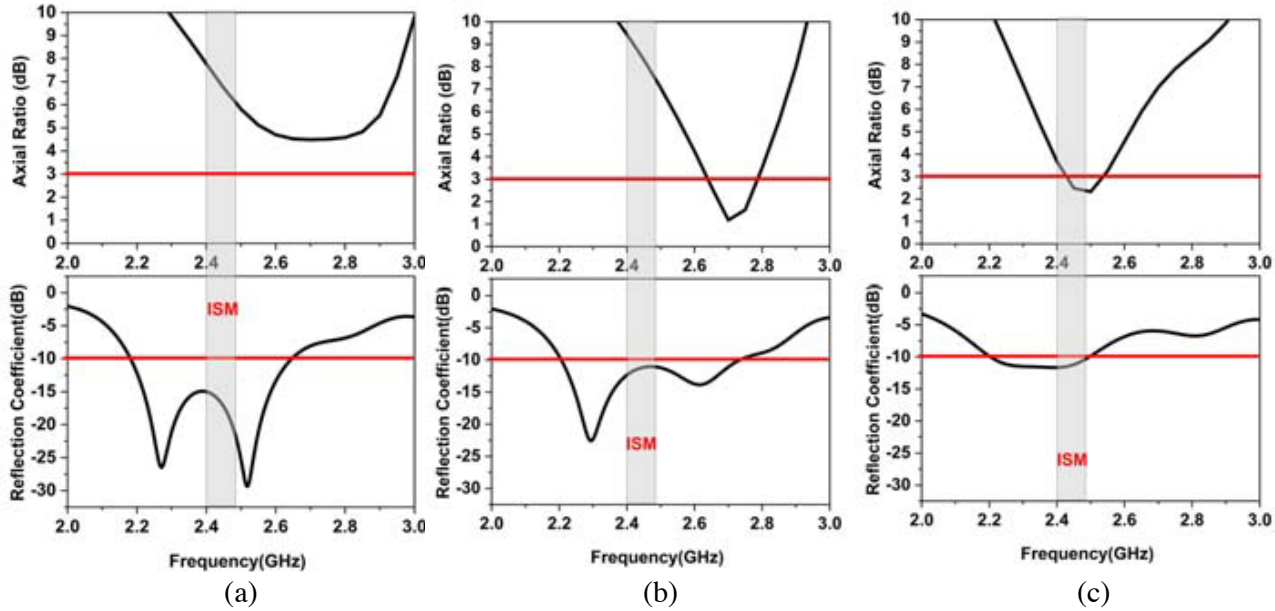

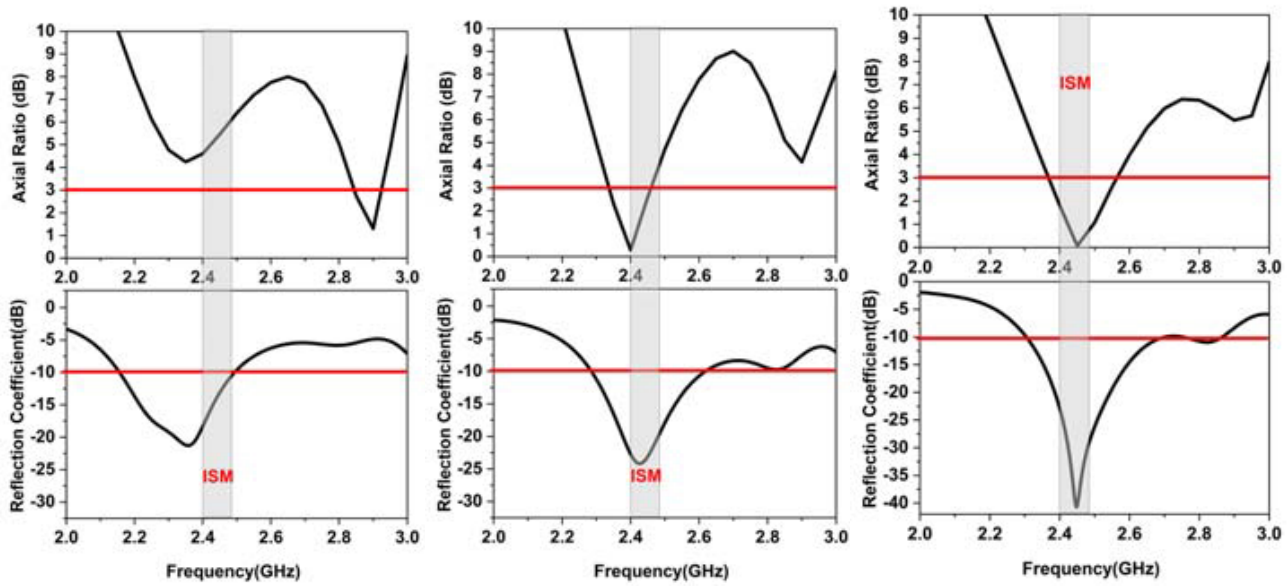

Figure 7. Reflection coefficients vs frequency and axial ratio vs frequency, (a) Stage-2, (b) $d = 20.15$ mm, (c) $h = 27$ mm, (d) $e = 3.5$ mm, (e) $l = 28.9$ mm, and (f) $f = 16$ mm (equivalent to Stage-3).

4.2. On-Body Performance

This section explains in details about the effects of high conductivity and permittivity towards the antenna performance degradation due to human body. Therefore, in order to account the effect, the back part of human body is considered, and the simulation is carried out by placing antennas of Stage-1, 2, 3, and 4 on a rectangular human body model. The model consists of skin, muscle, and fat, and their dielectric properties are tabulated in Table 4.

Table 4. Properties of rectangular human body model at 2.45 GHz [31].

Layers	Thickness (mm)	Permittivity	Conductivity (S/m)	Mass densities (kg/m^3)
Dry skin	2	38.007	1.4640	1090
Fat	8	5.280	0.1045	930
Muscle	23	52.729	1.7388	1050

When Stage-1 is placed on body model at '0 mm' distance, the reflection coefficient is degraded as shown in Figure 5(a). The 3-dB axial ratio is also changed; however, it resonates at 2.45 GHz ISM band (See Figure 6(a)). A reduced peak gain of -7 dBi and radiation efficiency of 3% are obtained as shown in Figure 8. On the contrary, with the presence of AMC in Stage-2, the antenna retains its impedance bandwidth to 440 MHz (2.18–2.62) with an improved gain of 7.1 dBi and efficiency of 77%. The same scenario is observed in Stage-3, and Stage-4 for on-body as compared to free space performance. Stage-3 provides an impedance bandwidth of 430 MHz with an improved gain of 7.4 dBi and a radiation efficiency of 76%. After the reduction of overall foot prints in Stage-4, the impedance bandwidth, gain, and efficiency of 350 MHz (2.34–2.69 MHz), 6.1 dBi, and 67% are obtained, respectively. The AR bandwidth retains its value same as free space in Stage-3 and Stage-4. The antenna characteristics of Stage-1, 2, and 3 in free space and on-body are tabulated in Table 5.

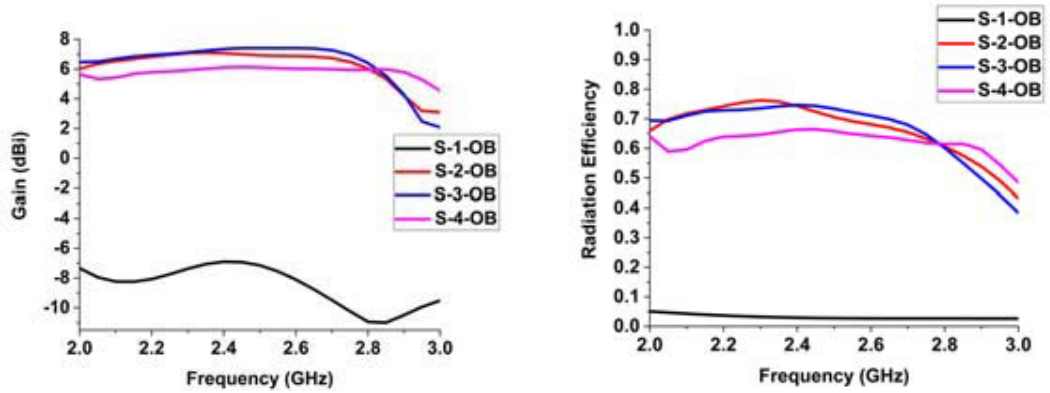

(a) (b)

Figure 8. (a) Realized gain on body, and (b) radiation efficiency on body for Stage-1 (S-1), Stage-2 (S-2), Stage-3 (S-3), and Stage-4 (S-4).

Table 5. Antenna performances in free space and on body.

Antenna	BW (MHz) FS/OB	Radiation efficiency (%) @2.45 GHz FS/OB	Gain (dBi) FS/OB	3-dB AR BW (MHz) FS/OB
Stage-1	310/degraded	80/3	1.6/−7	830/830
Stage-2	480/440	78/77	7.3/7.1	0/0
Stage-3	430/430	76/75	7.7/7.4	190/190
Stage-4	350/350	68/67	6.5/6.1	170/170

4.3. SAR Analysis

The amount of electromagnetic power absorbed per unit mass of tissue is defined as SAR expressed by Eq. (1).

$$\text{SAR} = \frac{\sigma \left| E^2 \right|}{\rho} \text{ (W/kg)} \tag{1}$$

where σ and ρ represent conductivity and mass density, respectively [36]. In this work, the SAR value is evaluated over the average of 1 g and 10 g tissues at 2.45 GHz with an input power (IP) of 0.1 W. The SAR distributions for stage-1, Stage-2, and Stage-4 are shown in Figure 9. The SAR values obtained by placing the antennas at 0 mm distance from the body are tabulated in Table 6. It is observed that the 1 g and 10 g SARs for Stage-1 are 4.63 and 1.9 W/kg, respectively. The reason for obtaining high value of SAR is due to significant backward radiation generating from omnidirectional patterns of antenna in Stage-1. On the contrary, with the presence of 3×3 AMC in Stage-2, the SAR is reduced by 99.47% (0.0245 W/kg) for 1 g tissue and 99.29% (0.0134 W/kg) for 10 g tissue. In Stage-3, the SAR reduction is furthermore improved to 99.63% (0.0171 W/kg) for 1 g tissue and 99.46% (0.0101 W/kg) for 10 g tissue. In Stage-4, by the implementation of 2×2 AMC, the SAR is reduced by 97.72% (0.106) for 1 g tissue and 96.6% (0.0646) for 10 g tissue. Thus, the proposed antenna provides the SAR value within the defined FCC limit.

4.4. Circular Polarization Mechanism

Figure 10 shows the mechanism of circular polarization with the help of surface current orientation at different phases (0°, 90°, 180°, 270°), and the principle reported in [30] is adopted to determine the state of polarization. From the figure it is observed that the dominant component of surface currents is

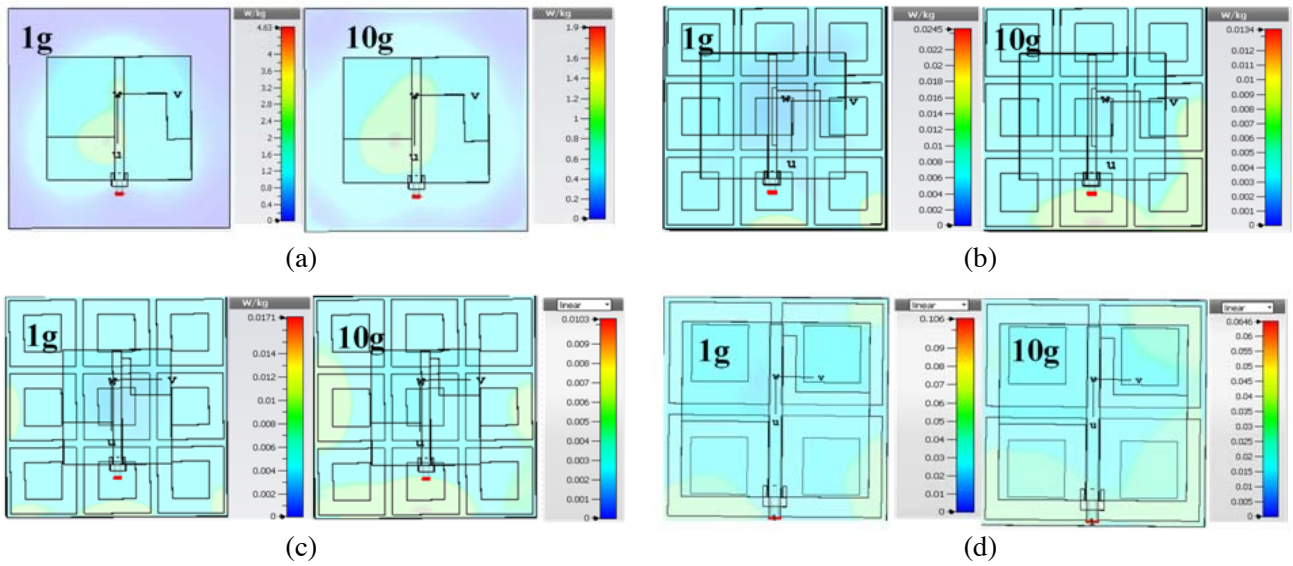

Figure 9. SAR distribution over 1 g and 10 g of tissues (a) Stage-1, (b) Stage-2, (c) Stage-3, and (d) Stage-4.

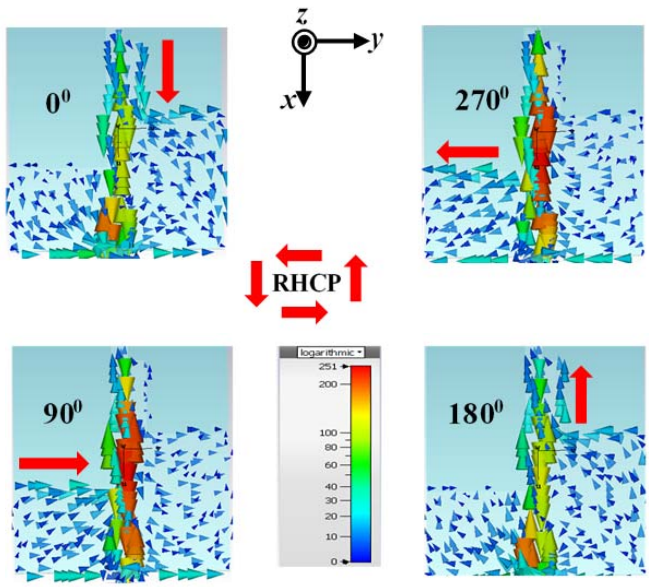

Figure 10. Surface current distribution of Stage-4 at different phases 0°, 90°, 180°, and 270°) and the principle reported in [30] is adopted to determine the state of polarization.

oriented along the x-directions at the stub's periphery, along the y-direction at the edge of ground plane for the phases of 0° and 90°, respectively. Similarly, for the phases 180° and 270°, the orientations of dominant components are along $-x$-direction and $-y$-direction, respectively. The dominant component of surface currents rotates anticlockwise to the direction of propagation with the progression of phase from 0°–90°–180°–270°. The same scenario is also observed from the surface current orientation of AMC plane. From the surface current distributions, it is observed that the vertical stub and horizontal edge of ground plane contribute to inducing the orthogonal components of equal amplitude which results in circular polarization. Thus, such behavior from the orientation of surface current confirms the existence of right handed circular polarization (RHCP).

Table 6. Simulated SAR at 2.45 GHz with input power 0.1 W for Stage-1, 2, 3, and 4 on the body at '0 mm' distance.

Antenna	1 g (W/kg)	10 g (W/kg)
Stage-1	4.63	1.9
Stage-2	0.0245	0.0134
Stage-3	0.0171	0.0101
Stage-4	0.106	0.0646

4.5. Bending Evaluation

In this section, the deformation performances of antennas are analyzed by bending the integrated antenna presented in Stage-4 with variant diameters of 70 mm, 80 mm, 100 mm, and 140 mm along x-axis and y-axis. The bending of integrated antenna is performed for ensuring the sustainability of operating frequency bandwidth. From Figure 11, it is observed that the resonant frequency and impedance bandwidth under bending retain their values the same as flat scenario.

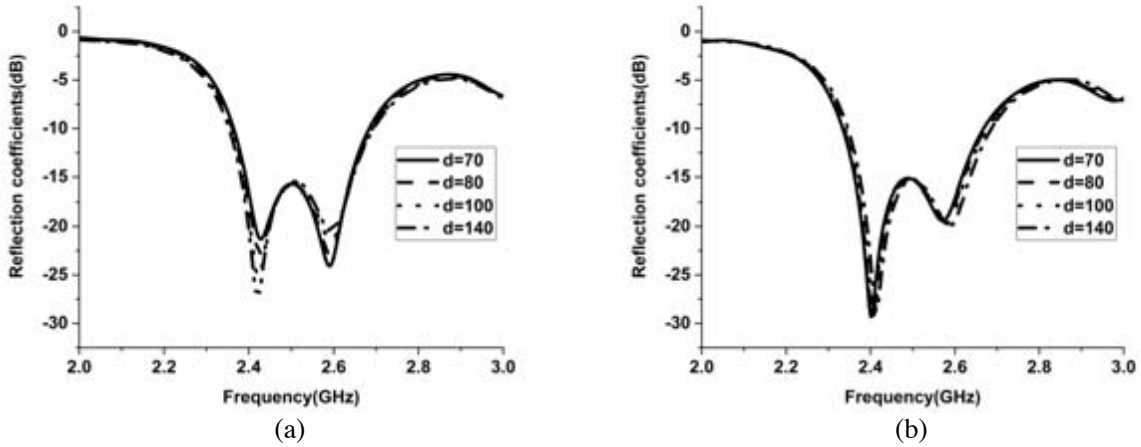

Figure 11. Simulated reflection coefficient (S_{11}) of antenna presented in Stage-4 for different bending diameters (mm) at the (a) x-axis, (b) y-axis.

4.6. Validation of Measured Results with Simulated Results

The proposed antenna presented in Stage-4 was fabricated using photo-lithographic method and hand-cutting tools to validate experimentally as shown in Figure 12. The reflection coefficient of fabricated antenna is measured using Agilent Vector network analyzer (VNA) for the frequency range from 1 GHz to 4 GHz as illustrated in Figure 13. The simulated antenna provides an impedance bandwidth of 350 MHz (2.35 GHz–2.7 GHz) with reflection coefficient's dip of −28.5 dB at 2.41 GHz, whereas the measured one is 580 MHz with dip −44.3 dB at 2.56 GHz. The reason of wider measured bandwidth might be due to the use of hand-cutting tools [36] and resonant frequency shifting might be due to slight variation of dielectric constant.

The simulated and measured axial ratio and gain vs frequency graphs are shown in Figures 14(a), and (b), respectively. Circular polarization was measured by rotating a linearly polarized horn antenna in E- and H-planes. The horn antenna was used as the transmitting antenna and the proposed antenna as the receiving antenna. Similarly, gain was measured within an anechoic chamber using a horn antenna at transmitting section and the antenna under test (proposed antenna) at receiving section. The distance between transmitting and receiving antennas was kept as 1 m. Then the gain of antenna under test was determined from the recorded receiving power, gain of horn antenna, and power of horn antenna. The

(a) (b)

Figure 12. Fabricated antenna, (a) front view, (b) back view.

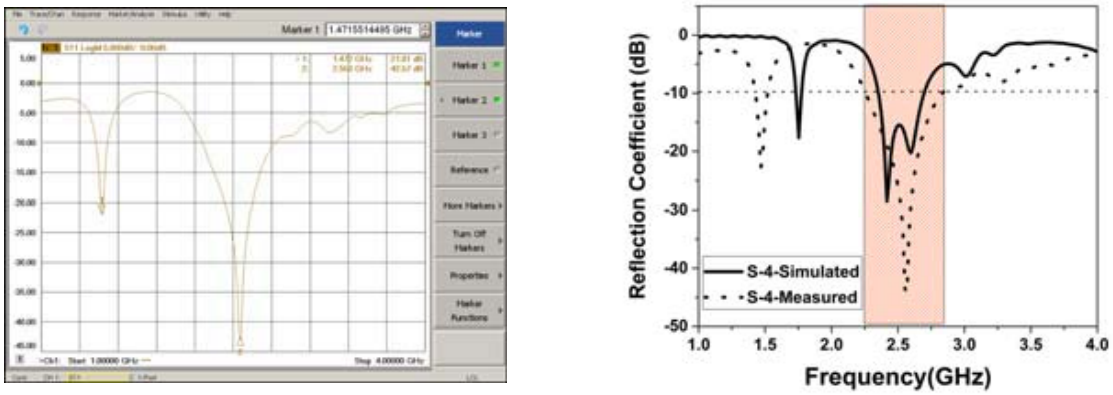

(a) (b)

Figure 13. (a) Reflection coefficients from VNA, (b) comparisons of measured and simulated reflection coefficients.

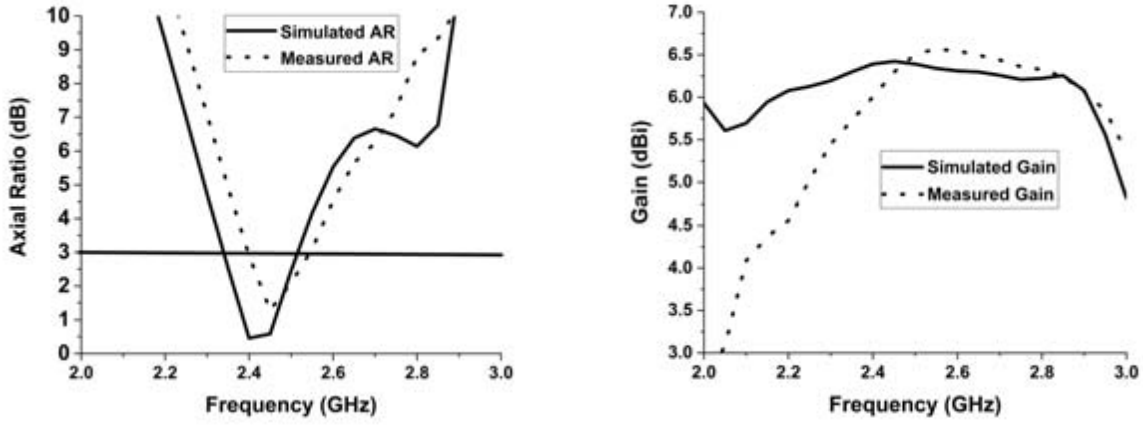

(a) (b)

Figure 14. Comparison of measured with simulated (a) axial ratio, (b) gain vs. frequency.

measured 3-dB operating AR BW is shifted slightly to right side with 150 MHz (2.39 GHz–2.54 GHz) as compared to simulation. A simulated peak gain of 6.5 dBi is obtained at 2.45 GHz, whereas the measured one is 6.6 dBi at 2.54 GHz.

Figure 15 depicts the simulated and measured RHCP and left-hand circular-polarization (LHCP) in x-z and y-z planes at 2.45 GHz. From the radiation plots, it is observed that in the broadside direction, the strengths of the simulated RHCP are 36 dB and 35 dB stronger than LHCP in the x-z and y-z planes, respectively, whereas the measured strengths of RHCP are 27 dB and 25.2 dB stronger than LHCP in the x-z and y-z planes, respectively. The measured co-polarization and cross-polarization are slightly less than simulated one because of shifting of AR dip towards upwards. From the above result and discussions, it is revealed that the proposed structure can be used for WBAN OFF-body communication at 2.4 GHz ISM band.

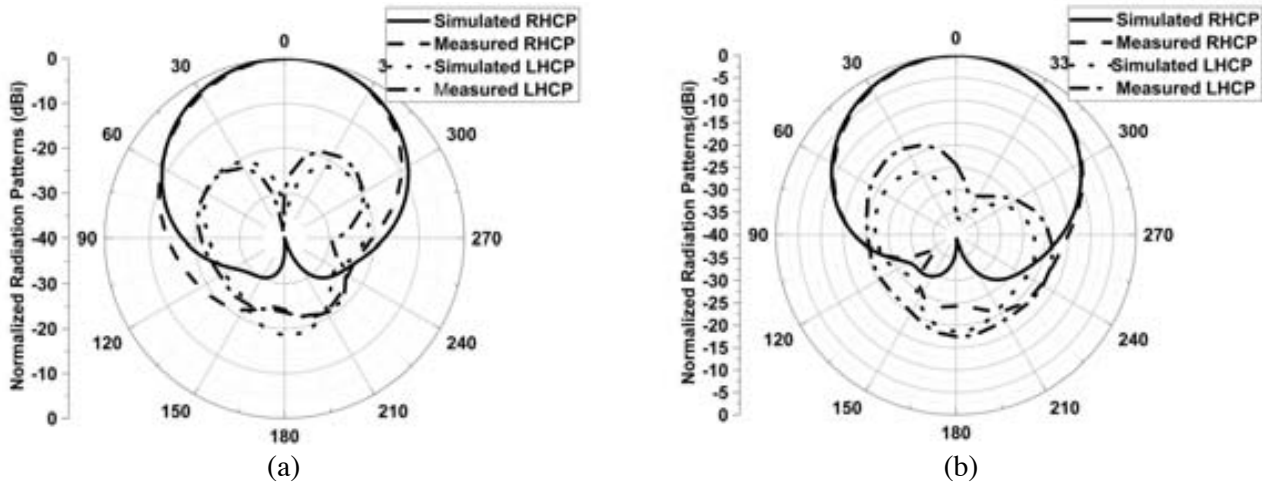

Figure 15. Measured and simulated RHCP and LHCP in (a) x-z plane, (b) y-z plane.

Table 7. Comparisons of previous works with present works.

Ref.	Op. Freq. (GHz)/BW(%)	Pol./AR BW (MHz)	Gain (dBi) /η (%)	Total Foot prints (λ_g^2@2.45 GHz)
[33]	2.45/5.5	LP/NA	1.94/73.6	0.82
[19]	2.45/4.44	LP/NA	6.01/51.36	1.32
[35]	2.4/3.8	LP/NA	4.04/NA	0.52
[31]	2.45/6.3	LP/NA	4.077/38.84	0.46
[32]	2.45/15.7	LP/NA	2.45/53	0.24
[34]	2.48/3.4	LP/NA	5.6/NA	0.86
[7]	2.45/16.66	LP/NA	8.55/71	3.09
[4]	2.4/27	LP/NA	NA/NA	0.25
[36]	2.45/4	LP/NA	6.4/NA	1.57
[12]	2.4/10.72	CP/69	5.2/68	0.47
Proposed work (Stage-3)	2.45/16.47	CP/190	7.23/77	0.88
Proposed work (Stage-4)	2.45/11.1	CP/120	6.1/68	0.39

4.7. Comparison with Other Literature

The comparisons of proposed antenna with existing literature are tabulated in Table 7 and Table 8. Table 7 presents the comparison in terms of impedance bandwidth, 3-dB axial bandwidth, gain, radiation efficiency, and total foot prints. Because the SAR is dependent upon IP and distance of antenna from body, here the SAR is evaluated using the corresponding IP and distance from the body as described in the existing literature and then compared.

Table 8. Comparisons of previous works with present works in terms of SAR.

Ref.	G_{a-b} (mm)/IP (W)/Freq.	SAR 1 g/10 g (W/kg)	SAR of Proposed Stage-3 1 g/10 g (W/kg)	SAR of Proposed Stage-4 1 g/10 g (W/kg)
[33]	10/0.5/2.45	NA/0.057	0.0581/0.0376	0.676/0.493
[19]	5/0.5/2.45	2.27/0.44	0.0682/0.0452	0.494/0.383
[35]	3/0.1/2.4	NA/0.09	0.0154/0.0103	0.0847/0.0572
[31]	3/0.1/2.45	0.0219/0.00719	0.0149/0.0101	0.0794/0.0531
[32]	5/0.2/2.45	NA/0.65	0.0273/0.0181	0.198/0.153
[34]	5/0.1/2.48	0.0536/0.0296	0.0132/0.00881	0.0894/0.0701
[7]	3.6/12.45	0.33/0.136	0.145/0.0973	0.743/0.599
[4]	1/0.1/2.4	0.0368/0.0138	0.0165/0.0111	0.106/0.0569
[36]	1/0.1/2.45	0.29/NA	0.0175/0.0112	0.0988/0.0537
[12]	4/0.1/2.4	0.13/NA	0.0147/0.00972	0.092/0.0729

5. CONCLUSION

A circularly polarized CPW fed monopole antenna with low SAR, high gain, high efficiency, and compact structure is presented for the 2.4 GHz ISM band. The antenna in Stage-4 provides all characteristics, followed by the evolution of Stage-1, Stage-2, and Stage-3. Initially, Stage-1 performed poorly in terms of impedance bandwidth, gain, radiation efficiency, and SAR on the body due to its omnidirectional radiation patterns. On the other hand, the performances are improved in Stage-2 by implementing a 3×3 AMC. However, as the AR curve shifted upward, the monopole antenna is optimized in Stage-3, resulting in additional SAR reduction and peak gain increment. Finally, the 2×2 AMC in Stage-4 contributed to reducing the overall footprints and SAR by 55.56% and 97.72%, respectively. On the body, it provided an impedance bandwidth, radiation efficiency, peak gain, 3-dB AR bandwidth of 350 MHz, 67%, 6.1 dBi, and 170 MHz, respectively. The fabricated antenna of Stage-4 provided an impedance bandwidth of 580 MHz, peak gain of 6.5 dBi, and 3 dB AR BW of 150 MHz. Based on the evolution of performance from Stage-1 to Stage-4, it can be concluded that increasing the size of reflector in comparison to the monopole antenna reduces SAR and increases peak gain. The proposed antenna could be a viable candidate for OFF-body communication application.

REFERENCES

1. Peter, S. H. and H. Yang, *Antennas and Propagation for Body-centric Wireless Communications*, Artech House, Noorwood, MA, USA, 2012.
2. Gareth, A. C. and G. S. William, "Antennas for over body surface communication at 2.45 GHz," *IEEE Trans. Antennas Propag.*, Vol. 57, No. 4, 844–855, 2009.
3. Linda, A. Y. P., J. S. Ping, and Y. Sen, "A high fidelity all textile UWB antenna with low back radiation for off-body WBAN applications," *IEEE Trans. Antennas Propag.*, Vol. 64, No. 2, 757–760, 2016.

4. Adel, Y. I. A., Z. A. Zuhairiah, and H. D. Samsul, "Compact and low profile textile EBG-based antenna for medical wearable applications," *IEEE Antennas Wireless Propag. Lett.*, Vol. 14, 2550–2553, 2017.
5. Sen, Y., J. S. Ping, and A. E. V. Guy, "Low-profile dual-band textile antenna with artificial magnetic conductor plane," *IEEE Trans. Antennas Propag.*, Vol. 62, No. 12, 6487–6490, 2014.
6. Sangeetha, V. and F. S. Malathi, "Dual-band EBG integrated monopole antenna deploying fractal geometry for wearable applications," *IEEE Antennas Wireless Propag. Lett.*, Vol. 14, 249–252, 2015.
7. Alemaryeen, A. and S. Noghanian, "Crumpling effects and specific absorptions rate of flexible AMC integrated antennas," *IET Microw. Antennas Propag.*, Vol. 12, No. 4, 627–635, 2018.
8. Natale, A. D. and E. D. Giampaolo, "A reconfigurable all-textile wearable UWB antenna," *Progress In Electromagnetic Research C*, Vol. 106, 31–43, 2020.
9. Osman, M. A. R., M. K. A. Rahim, N. A. Samsuri, H. A. M. Salim, and M. F. Ali, "Embroidered full textile wearable antenna for medical monitoring applications," *Progress In Electromagnetics Research*, Vol. 117, 321–337, 2011.
10. Balarami Reddy, B. N., P. Sandeep Kumar, T. Rama Rao, N. Tiwari, and M. Balachary, "Design and analysis of wideband monopole antennas for flexible/wearable wireless device applications," *Progress In Electromagnetics Research M*, Vol. 62, 167–174, 2017.
11. Sherif, R. Z., A. A. Mahmoud, and G. Abdelhamid, "New thin wide-band bracelet-like antenna with low SAR for on-arm WBAN applications," *IET Microw. Antennas Propag.*, Vol. 13, No. 8, 1219–1225, 2019.
12. Jiang, Z. H., C. Zheng, and T. Yue, "Compact, highly efficient, and fully flexible circularly polarized antenna enabled by silver nanowires for wireless body-area networks," *IEEE Trans. Biomed. Curcuits Syst.*, Vol. 11, No. 4, 920–932, 2017.
13. Muhammad, A. B. A., S. N. Symeon, and A. A. Macro, "Compact EBG-backed planar monopole for BAN wearable applications," *IEEE Trans. Antennas Propag.*, Vol. 65, No. 2, 453–463, 2017.
14. Zhi, H. J., E. B. Donovan, and E. S. Peter, "A Compact low-profile meta-surface enabled antenna for wearable medical body-area network devices," *IEEE Trans. Antennas Propag.*, Vol. 62, No. 8, 4021–4030, 2014.
15. Haider, R. K., I. A. Ayman, and M. A. Hussain, "Analysis of radiation characteristics of conformal arrays using adaptive integral method," *IEEE Trans. Antennas Propag.*, Vol. 61, No. 2, 524–531, 2013.
16. Simone, G., C. Filippo, and F. Filippo, "Wearable inject-printed wideband antenna by using miniaturized AMC for sub-GHz applications," *IEEE Antennas Wireless Propag. Lett.*, Vol. 15, 1927–1930, 2016.
17. Mohamed, E., A. A. Mohmoud, and M. E. Hadia, "Gain enhancement of a compact thin flexible reflector-based asymmetric meander line antenna with low SAR," *IET Microw. Antennas Propag.*, Vol. 12, No. 4, 627–635, 2018.
18. Mohamed, E., A. A. Mahmoud, and M. E. Hadia, "A wearable dual-band low profile high gain low SAR antenna AMC backed for WBAN application," *IEEE Trans. Antennas Propag.*, Vol. 67, No. 10, 6378–6388, 2019.
19. Wang, M., Z. Yang, and J. Wu, "Investigation of SAR reduction using flexible antenna with meta material structurein wireless body area network," *IEEE Trans. Antennas Propag.*, Vol. 66, No. 6, 3076–3086, 2018.
20. Abirami, B. S. and F. S. Esther, "EBG-backed flexible printed Yagi-Uda antenna for on-body communication," *IEEE Trans. Antennas Propag.*, Vol. 65, No. 7, 3762–3765, 2017.
21. Sangkil, K., J. R. Yu, and L. Hoseon, "Monopole antenna with inject-printed EBG array on paper substrate for wearable applications," *IEEE Antennas Wireless Propag. Lett.*, Vol. 11, 663–666, 2012.
22. Benjamin, S. C. and S. Atif, "Utilizing wide band AMC structures for high-gain inject printed antennas on lossy paper substrate," *IEEE Antennas Wireless Propag. Lett.*, Vol. 12, 76–79, 2013.

23. Benjamin, S. C. and S. Atif, "Wearable AMC backed near-endfire antenna for on-body communications on latex substrate," *IEEE Trans. Compon. Packag. Manuf. Technol.*, Vol. 6, No. 3, 346–358, 2016.
24. Means, D. L. and K. W. Chan, "Evaluating compliance with FCC guidelines for human exposure to radiofrequency electromagnetic fields," Office of Engineering and Technology Federal Communication Commission FCC, Washington D.C., 2001.
25. "Commision implementing decision (EU) 2016/537," *Official Journal of the European Union*, 2016.
26. Faruqque, M. R. I., M. I. Hossain, and M. T. Islam, "Low specific absorption rate microstrip patch antenna for cellular phone applications," *IET Microw. Antennas Propag.*, Vol. 9, No. 14, 1540–1546, 2015.
27. Roy, B. V. B. S., K. Asimina, and P. E. Karu, "UWB wearable antenna with full ground plane based on PDMS-embedded conductive fabric," *IEEE Antennas Wireless Propag. Lett.*, Vol. 17, No. 3, 493–496, 2018.
28. Hertleer, C., H. Rogier, L. Vallozzi, and L. van Langenhove, "A textile antenna for off-body communication integrated into protective clothing for firefighters," *IEEE Trans. Antennas Propag.*, Vol. 57, No. 4, 919–925, 2009.
29. Locher, I., M. Klemm, T. Kirstein, and G. Troster, "Design and characterization of purely textile patch antennas," *IEEE Trans. Adv. Packag.*, Vol. 29, No. 4, 777–788, 2006.
30. Ullah, U., I. B. Mabrouk, and S. Koziel, "A compact circularly polarized antenna with directional pattern for wearable off-body communications," *IEEE Antennas Wireless Propag. Lett.*, Vol. 18, 2523–2527, 2019.
31. Atrash, M. E., O. F. Abdalgalil, I. S. Mamoud, M. A. Abdalla, and S. R. Zahran, "Wearable high gain low SAR antenna loaded with backed all-textile EBG for WBAN applications," *IET Microw. Antennas Propag.*, Vol. 14, No. 8, 791–799, 2020.
32. Zhang, K. and G. A. E. Vandenbosch, "A novel design approach for compact wearable antennas based on metasurfaces," *IEEE Trans. Antennas Propag.*, Vol. 14, No. 4, 918–927, 2020.
33. Joshi, R., E. F. N. M. Hussin, P. J. Soh, M. F. Jamlos, H. Lago, A. A. A. Hadi, and S. K. Podilchak, "Dual-band, dual-sense textile antenna with AMC backing for localization using GPS and WBAN/WLAN," *IEEE Access*, Vol. 8, 89468–89478, 2020.
34. Gao, G., R. Zhang, C. Yang, H. Meng, W. Geng, and B. Hu, "Microstrip monopole antenna with a novel UC-EBG for 2.4 GHz WBAN applications," *IET Microw. Antennas Propag.*, Vol. 13, No. 13, 2319–2323, 2019.
35. Balakrishnan, S. A. and E. F. Sudarsingh, "Conformal self-balanced EBG integrated printed folded dipole antenna for wireless body area networks," *IET Microw. Antennas Propag.*, Vol. 13, No. 14, 2480–2485, 2019.
36. Saeed, S. M., C. A. Balanis, C. R. Birtcher, A. C. Durgun, and H. N. Shaman, "Wearable flexible reconfigurable antenna integrated with artificial magnetic conductor," *IEEE Antennas Wireless Propag. Lett.*, Vol. 16, 2396–2399, 2017.
37. Yun, S., D. Y. Kim, and S. Nam, "Folded cavity-backed crossed-slot antenna," *IEEE Antennas Wireless Propag. Lett.*, Vol. 14, 36–39, 2015.
38. Lui, K. W., O. H. Murphy, and C. Toumazou, "A wearable wideband circularly polarized textile antenna for effective power transmission on a wireless-powered sensor platform," *IEEE Trans. Antennas Propag.*, Vol. 61, No. 7, 3873–3876, 2013.
39. Kaivanto, E. K., M. Berg, E. Salonen, and P. de Maagt, "Wearable circularly polarized antenna for personal satellite communication and navigation," *IEEE Trans. Antennas Propag.*, Vol. 59, No. 12, 4490–4496, 2011.
40. Ismail, M. F., M. K. A. Rahim, E. I. S. Saadon, and M. S. Mohd, "Compact circularly polarized textile antenna," *Proc. 2014 IEEE Symp. Wireless Tech. Appl.*, 134–136, Oct. 2014.
41. Specification Sheet-Felt Sheet RS Component Inc., 2013.